Ag@SiO$_2$ Core−Shell Nanoparticles for Probing Spatial Distribution of Electromagnetic Field Enhancement *via* Surface-Enhanced Raman Scattering

Wei Wang,[†] Zhipeng Li,[‡] Baohua Gu,[†,]* Zhenyu Zhang,[§,‖] and Hongxing Xu[‡,⊥,]*

[†]Environmental Sciences, [§]Materials Science & Technology Divisions, Oak Ridge National Laboratory, Oak Ridge, Tennessee 37831, [‡]Beijing National Laboratory for Condensed Matter Physics, Institute of Physics, Chinese Academy of Sciences, Beijing 100190, China, [‖]Department of Physics and Astronomy, University of Tennessee, Knoxville, Tennessee 37996, and [⊥]Division of Solid State Physics, Lund University, Box 118, S-22100, Sweden

S urface-enhanced Raman scattering (SERS) has received increasing attention in recent years because of its high sensitivity in detecting and characterizing a wide range of chemical and biological agents up to single molecular concentration levels.[1−4] SERS has been attributed to both electromagnetic (EM)[5−7] and chemical enhancements,[7−9] although exact mechanisms of the EM enhancement at roughened metal surfaces or nanoparticles are not yet fully understood on a quantitative level. Both experimental evidence and theoretical simulations indicate that maximum SERS enhancement occurs when analyte molecules are located near the surface or in the nanogap regions of metal nanoparticles.[7,10,11] In particular, the enhancement region has been predicted to attenuate rapidly within a few nanometers away from the metal surfaces but experimental verification of this prediction has been scarce and difficult. Previous studies relied on the use of molecular spacers,[12−14] but changes in the molecular size and chemical property of different molecules can lead to changes of the EM enhancement and thus make it challenging to determine the true spatial distribution of the local EM field. Recent studies using a series of laser pulses to burn away molecules at sites with progressively decreasing EM fields enabled the determination of the spatial distribution of the "hot" and "cold" SERS sites,[15] but further understanding of the site enhancement demands precise determination of the distance-dependent changes of the EM fields.

ABSTRACT We show that the spatial distribution of the electromagnetic (EM) field enhancement can be probed directly *via* dynamic evolution of surface-enhanced Raman scattering (SERS) of rhodamine 6G (R6G) molecules as they diffuse into Ag@SiO$_2$ core−shell nanoparticles. The porous silica shell limits the diffusion of R6G molecules toward inner Ag cores, thereby allowing direct observation and quantification of the spatial distribution of SERS enhancement as molecules migrate from the low to high EM fields inside the dielectric silica shell. Our experimental evidence is validated by the generalized Mie theory, and the approach can potentially offer a novel platform for further investigating the site and spatial distribution of the EM fields and the EM *versus* chemical enhancement of SERS due to molecular confinement within the Ag@SiO$_2$ nanoshell.

KEYWORDS: Raman scattering · nanoparticles · silver · silica · spatial distribution · electromagnetic field enhancement

In this paper, we provide a combined experimental and theoretical study of the dynamic evolution of the EM field enhancement *via* SERS in both time and space as rhodamine 6G (R6G) molecules diffuse into the porous Ag@SiO$_2$ core−shell nanoparticles. The nanoporous structure of the SiO$_2$ shell hinders the diffusion of R6G molecules toward the inner Ag metal cores, thereby allowing direct observation and quantification of the dynamic and spatial distribution of SERS enhancement as R6G molecules migrate from the low to high EM enhancement regions inside the dielectric SiO$_2$ shell. The research demonstrates that Ag@SiO$_2$ nanoshells could serve as a novel platform for further studies of the site and spatial distribution of the EM fields and the EM *versus* chemical enhancement of SERS due to molecular confinement.

RESULTS AND DISCUSSION

The Ag@SiO$_2$ core−shell nanoparticles were synthesized by hydrolysis of tetraethyl orthosilane (TEOS) in microemulsion.[16]
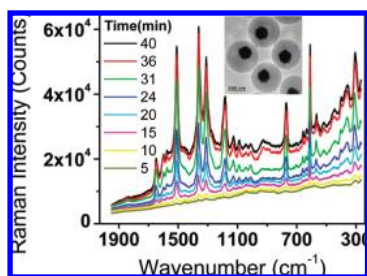
Figure 1. Dynamic evolution of SERS spectra of R6G (5 × 10^{-6} M) from Ag@SiO$_2$ core−shell nanoparticle substrates. Only selected spectra were plotted without baseline corrections for better clarity (additional spectra provided in Supporting Information). Laser power, ~1.5 mW at 785 nm and integration time, 10 s. Inset: TEM image of synthesized Ag@SiO$_2$ core−shell nanoparticles with an Ag core radius of about 70 nm and SiO$_2$ shell thickness of about 115 nm.

Transmission electron microscopy (TEM) provided clear images of Ag cores with an average radius of about 70 nm and SiO$_2$ shells with an average thickness of about 115 nm (Figure 1 inset). The SiO$_2$ nanoparticles made by the afore-mentioned synthetic technique are porous with pore diameters about 1−3 nm,[17−19] which allows for molecular diffusion of R6G through the SiO$_2$ shell since R6G has a dimension of about 0.8 × 1.6 nm.[20,21] In comparison with pure Ag particles (without SiO$_2$ shells), the plasmon absorption maximum of the Ag@SiO$_2$ composite nanoparticles red-shifted to about 502 nm (Supporting Information, Figure S1) owing to the size of the Ag core and a relatively high refractive index of the SiO$_2$ shell.[22] Time-dependent SERS spectra were subsequently collected directly from a suspension containing Ag@SiO$_2$ nanoparticles and R6G (5 × 10^{-6} M) as a probing molecule. The sample was placed in a sealed quartz cell to prevent water from evaporation during spectral collections.

Figure 1 shows a typical set of SERS spectra collected at different time intervals. Within the first 10 min, SERS signals of R6G were hardly observable. While the signature of R6G could be noted, spectra collected at 2, 5, 7, and 10 min were essentially the same, suggesting that R6G molecules were probably too far from the Ag surface to exhibit strong SERS. However, the SERS signal increased about 10 min after mixing the nanoparticles with R6G in water. It increased monotonically up to about 40 min as R6G molecules approached the Ag cores and finally became saturated with further increasing the reaction time. Since the measurement was performed in aqueous suspension in a closed quartz cell, the observed dynamic increase in SERS intensity could not be explained by the drying or concentration effect of the sample. It cannot be explained by an increased adsorption or concentration of R6G on Ag surfaces either because the fluorescence intensity of the sample remains unchanged over time. The sorption of R6G mol-

ecules on Ag would otherwise cause significant quenching or a decreased fluorescence such as on bare Ag nanoparticles under the same experimental conditions (Supporting Information, Figure S3). On the other hand, the observed phenomena could be well explained by spatially distributed EM fields or SERS enhancement sites in the SiO$_2$ nanoshell due to the surface plasmon excitation of Ag cores. A slow migration or diffusion of R6G molecules through the local field resulted in a time-dependent increase of the Raman scattering signal because SERS is known to depend on the location of analyte molecules at the close proximity of metal nanoparticle surfaces, with maximum SERS enhancement expected only when analyte molecules are situated a few nanometers away from the nanoparticle surface or within the nanoneck of adjacent metal nanoparticles.[7,23]

The above rationale is supported by model simulations within the generalized Mie theory. On the basis of the time or spatial-dependent SERS enhancement, the diffusion coefficient of R6G within the confined SiO$_2$ nanoporous structure is obtained by solving the following diffusion equation:[24]

$$\frac{\partial C(r,t)}{\partial t} = D\frac{1}{r^2}\frac{\partial}{\partial r}\left(r^2\frac{\partial C(r,t)}{\partial r}\right) \tag{1}$$

where D is the effective diffusion coefficient, C is the concentration of R6G inside the SiO$_2$ shell, t is the time, and r is the radial coordinate. The average SERS enhancement factor (G_{ave}) around and within a homogeneous SiO$_2$ layer of a metal-dielectric nanosphere is given by integrating all Raman scattering contributions from the volume of the spherical shell (v):

$$G_{ave}(t) = \int_v G_{loc}(r)\, C(r,t)\, dV \tag{2}$$

where G_{loc} is the ratio between emitted scattering intensities of the analyte molecules in the presence and absence of Ag metal surfaces. It is estimated by $|E_{loc}(\mathbf{r},\omega_0)/E_0(\omega_0)|^4$, where E_0 is the incident electric field, $\mathbf{E}_{loc}$ is the local electric field at the position $\mathbf{r}$ of the dipole, and ω_0 is the incident frequency. Note that D is the only adjustable parameter used in calculations; the initial and
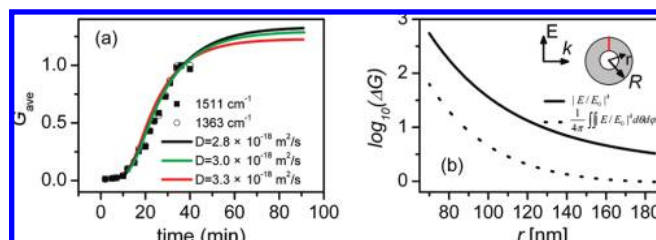

Figure 2. (a) Comparisons between experimentally observed (solid square and open circle) and theoretically predicted (lines) SERS enhancement factor, G_{ave}, using spectral data at 1511 or 1363 cm^{-1} in Figure 1. All data were normalized to the saturation value collected at 40 min. The estimated effective diffusion coefficient, D, is 2.8 × 10^{-18} to 3.3 × 10^{-18} m²/s. (b) The local EM intensity enhancement (ΔG) along the transect of the silica shell shown in the inset (solid line) and the averaged ΔG over the surface at radius r (dashed line).

boundary conditions are obtained from experimental data (additional details provided in Supporting Information). In particular, an initial 10-min delay was used, allowing R6G molecules to diffuse sufficiently close to the Ag core to exhibit the SERS signal (Figure 1).

A good agreement is obtained between theoretically calculated G_{ave} and experimentally observed values based on Raman bands at 1511 and 1363 cm^{-1} (Figure 2a). The G_{ave} increased as molecules diffuse into the enhanced local EM field at the close distance of Ag cores (Figure 2b).

After about 40 min, it reached a plateau, indicating the arrival of molecules in the "hottest" EM fields. The SERS intensity remained relatively stable thereafter (Supporting Information, Figure S2). The D value estimated from above calculations is about 2.8×10^{-18} to 3.3×10^{-18} m^2/s for the diffusion of R6G molecules within silica nanopores. This value is about 8 orders of magnitude lower than that observed in free water but is in agreement with that measured in silica nanochannels synthesized by similar sol−gel techniques.[25,26] Although this slow diffusion may also be caused by the potential sorption of R6G molecules within the SiO$_2$ nanopores,[27−29] it nonetheless demonstrates a profound impact of the confinement and interactions of molecules within silica nanopore structures on the diffusion of R6G. However, we note that the predicted arrival time appeared to be slightly longer than that observed experimentally. This is attributed to the fact that the shell thickness of synthesized Ag@SiO$_2$ nanoparticles is not homogeneous (Figure 1 inset), whereas both the core and the shell are treated as concentric spheres in model calculations. Molecules could thus reach to the "hottest" EM fields quicker than the theory would predict at the thinner part of the shell.

Figure 3a further illustrates the spatial distribution of the G_{loc} values in the SiO$_2$ nanoshell. The strongest SERS enhancement ($\sim10^3$) is found at the close proximity of the Ag core, but it attenuates radically with dis-
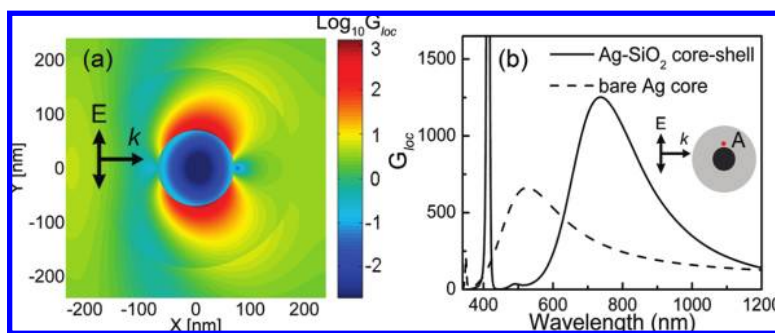

Figure 3. (a) Calculated spatial distribution of the enhancement factor (G_{loc}) on the wave plane, where the wave vector **k** and the polarization of incident light are denoted by arrows. The laser excitation wavelength is 785 nm. (b) Theoretically calculated G_{loc} values *versus* the incident wavelength at a given point A (denoted by a red dot), which is about 1 nm away from the surface of the Ag core. Optical constants of the shell and the medium are 1.44 and 1.33, respectively.

tance. In addition, the SERS enhancement in the core−shell nanostructure is found at its maximum at the incident wavelength of 785 nm and is higher than that by using bare Ag nanoparticles (Figure 3b). At the outer surface of the SiO$_2$ shell, a modest enhancement is also observed, but it attenuates radically again (Figure 3a). This result agrees with the fact that a weak but consistent signal of R6G could be seen within the first 10 min (Figure 1 and Supporting Information, Figure S2). In the absence of Ag@SiO$_2$ nanoparticles, no R6G signal could be detected at 5×10^{-6} M. Outside the silica shell, R6G molecules should be distributed evenly and therefore unlikely contribute to the time-dependent increase of SERS intensities shown in Figure 1.

This study thus concludes that the hindered diffusion of R6G molecules from the low to high SERS enhancement regions within confined SiO$_2$ nanoshells is responsible for the observed time-accumulation behavior of enhanced Raman scattering. This dynamic evolution of SERS predicted by the extended Mie theory allows the direct observation and quantification of the spatial distribution of SERS enhancement as molecules migrate from the low to high EM fields inside the dielectric SiO$_2$ shell.

METHODS

The Ag@SiO$_2$ core−shell nanoparticles were synthesized in water-in-oil microemulsion reaction medium (27.45 g Igepal CO-720, 22.0 mL hexanol, 170 mL cyclohexane, 10.7 mL 1 M AgNO$_3$ solution and 3.0 mL 29.5% NH$_3$H$_2$O).[16] Ag nanoparticles were first produced by reducing Ag(NH$_3$)$_2^+$ with 0.2 mL hydrazine (NH$_2$−NH$_2$) in the microemulsion, followed by the addition of 0.5 mL of 3-aminopropyltriethoxy silane (APS, as a coupling agent) and 9.5 mL of tetraethyl orthosilicate (TEOS) under vigorous stirring. The reaction was continued for 24 h for completion. The hydrolysis and condensation of the TEOS monomers catalyzed by ammonia allowed the growth of the SiO$_2$ shell surrounding Ag cores and the formation of spherical core−shell composite nanoparticles. These synthesized nanoparticles were collected from the microemulsion and purified by repeated washing with acetone, ethanol, and water. Finally the nanoparticle suspension was dialyzed against deionized water to remove soluble impurities until the electrical conductivity was <2

μS. The size of nanoparticles was determined by TEM (Hitachi HF 2000 transmission electron microscope operated at 200 kV). Absorption spectra of the sample were measured with a Hewlett-Packard 8453 spectrophotometer.

For SERS measurement, an aliquot of Ag@SiO$_2$ nanoparticle suspension (50 μL) was mixed with 4 mL of rhodamine 6G solutions at varying concentrations in sealed quartz cells. Time-dependent SERS spectra were recorded using a Renishaw micro-Raman system equipped with a 785-nm near-infrared diode laser (Renishaw Inc., New Mills, UK). The laser beam was set in position through a Leica Raman imaging microscope objective focused through the quartz window. About 1.5-mW laser power was used for the excitation. A charge coupled device (CCD) array detector was used to achieve signal detection from a 1200 g/mm grating light path controlled by Renishaw WiRE software and analyzed by Galactic GRAMS software. All spectra were recorded with a resolution of $\sim$2.5 cm^{-1} and 10 s accumulation. No baseline corrections were used for all the spectra.

Supporting Information Available: Extinction spectrum of Ag@SiO$_2$ core−shell nanoparticles, detailed time-dependent SERS spectra, R6G fluorescence, and theoretical calculations and parameters. This material is available free of charge *via* the Internet at http://pubs.acs.org.

REFERENCES AND NOTES

1. Moskovits, M.; Tay, L. L.; Yang, J.; Haslett, T. SERS and the Single Molecule. In *Optical Properties of Nanostructured Random Media*; Shalaev, V. M., Ed.; Springer: Berlin, 2002, pp 215−227.
2. Qian, X. M.; Nie, S. M. Single-Molecule and Single-Nanoparticle SERS: From Fundamental Mechanisms to Biomedical Applications. *Chem. Soc. Rev.* **2008**, *37*, 912–920.
3. Kneipp, J.; Kneipp, H.; Kneipp, K. SERS: A Single-Molecule and Nanoscale Tool for Bioanalytics. *Chem. Soc. Rev.* **2008**, *37*, 1052–1060.
4. Zeiri, L.; Bronk, B. V.; Shabtai, Y.; Eichler, J.; Efrima, S. Surface-Enhanced Raman Spectroscopy As a Tool for Probing Specific Biochemical Components in Bacteria. *Appl. Spectrosc.* **2004**, *58*, 33–40.
5. Kneipp, K.; Wang, Y.; Kneipp, H.; Itzkan, I.; Dasari, R. R.; Feld, M. S. Population Pumping of Excited Vibrational States by Spontaneous Surface-Enhanced Raman Scattering. *Phys. Rev. Lett.* **1996**, *76*, 2444–2447.
6. Nordlander, P.; Oubre, C.; Prodan, E.; Li, K.; Stockman, M. I. Plasmon Hybridizaton in Nanoparticle Dimers. *Nano Lett.* **2004**, *4*, 899–903.
7. Xu, H. X.; Bjerneld, E. J.; Käll, M.; Börjesson, L. Spectroscopy of Single Hemoglobin Molecules by Surface Enhanced Raman Scattering. *Phys. Rev. Lett.* **1999**, *83*, 4357–4360.
8. Sun, M. T.; Wan, S. B.; Liu, Y. J.; Jia, Y.; Xu, H. X. Chemical Mechanism of Surface-Enhanced Resonance Raman Scattering *via* Charge Transfer in Pyridine-Ag-2 Complex. *J. Raman Spectrosc.* **2008**, *39*, 402.
9. Lombardi, J. R.; Birke, R. L. Time-Dependent Picture of the Charge-Transfer Contributions to Surface Enhanced Raman Spectroscopy. *J. Chem. Phys.* **2007**, *126*, 244709.
10. Olk, P.; Renger, J.; Hartling, T.; Wenzel, M. T.; Eng, L. M. Two Particle Enhanced Nano Raman Microscopy and Spectroscopy. *Nano Lett.* **2007**, *7*, 1736–1740.
11. Gunnarsson, L.; Bjerneld, E. J.; Xu, H. X.; Petronis, S.; Kasemo, B.; Käll, M. Interparticle Coupling Effects in Nanofabricated Substrates for Surface-Enhanced Raman Scattering. *Appl. Phys. Lett.* **2001**, *78*, 802–804.
12. Kovacs, G. J.; Loutfy, R. O.; Vincett, P. S.; Jennings, C.; Aroca, R. Distance Dependence of SERS Enhancement Factor from Langmuir−Blodgett Monolayers on Metal Island Films—Evidence for the Electromagnetic Mechanism. *Langmuir* **1986**, *2*, 689–694.
13. Ye, Q.; Fang, J.; Sun, L. Surface-Enhanced Raman Scattering from Functionalized Self-Assembled Monolayers. 2. Distance Dependence of Enhanced Raman Scattering from an Azobenzene Terminal Group. *J. Phys. Chem. B* **1997**, *101*, 8221–8224.
14. Zou, S. Z.; Weaver, M. J. Surface-enhanced Raman Scattering an Uniform Transition Metal Films: Toward a Versatile Adsorbate Vibrational Strategy for Solid-Nonvacuum Interfaces. *Anal. Chem.* **1998**, *70*, 2387–2395.
15. Fang, Y.; Seong, N.-H.; Dlott, D. D. Measurement of the Distribution of Site Enhancements in Surface-Enhanced Raman Scattering. *Science* **2008**, *321*, 388–392.
16. Wang, W.; Asher, S. A. Photochemical Incorporation of Silver Quantum Dots in Monodisperse Silica Colloids for Photonic Crystal Applications. *J. Am. Chem. Soc.* **2001**, *123*, 12528–12535.
17. Kobler, J.; Möller, K.; Bein, T. Colloidal Suspensions of Functionalized Mesoporous Silica Nanoparticles. *ACS Nano* **2008**, *2*, 791–799.
18. Finnie, K. S.; Bartlett, J. R.; Barb, C. J. A.; Kong, L. Formation of Silica Nanoparticles in Microemulsions. *Langmuir* **2007**, *23*, 3017–3024.
19. Yu, J.; Zhao, L.; Cheng, B. Preparation of Monodispersed Microporous SiO$_2$ Microspheres with High Specific Surface Area Using Dodecylamine As a Hydrolysis Catalyst. *J. Solid State Chem.* **2006**, *179*, 226–232.
20. Sasai, R.; Fujita, T.; Iyi, N.; Itoh, H.; Takagi, K. Aggregated Structures of Rhodamine 6G Intercalated in a Fluor-Taeniolite Thin Film. *Langmuir* **2002**, *18*, 6578–6583.
21. Mubarekyan, E.; Santore, M. Characterization of Polystyrene Latex Surfaces by the Adsorption of Rhodamine 6G. *Langmuir* **1998**, *14*, 1597–1603.
22. Brandl, D. W.; Oubre, C.; Nordlander, P. Plasmon Hybridization in Nanoshell Dimers. *J. Chem. Phys.* **2005**, *123*, 024701.
23. Xu, H. X.; Aizpurua, J.; Käll, M.; Apell, P. Electromagnetic Contributions to Single-Molecule Sensitivity in Surface-Enhanced Raman Scattering. *Phys. Rev. E* **2000**, *62*, 4318–4324.
24. Crank, J. *The Mathematics of Diffusion*; Oxford University Press: New York, 1975.
25. Kievsky, Y. Y.; Carey, B.; Naik, S.; Mangan, N.; Ben-Avraham, D.; Sokolov, I. Dynamics of Molecular Diffusion of Rhodamine 6G in Silica Nanochannels. *J. Chem. Phys.* **2008**, *128*, 151102.
26. Fu, Q.; Rao, G. V. R.; Ista, L. K.; Wu, Y.; Andrzejewski, B. P.; Sklar, L. A.; Ward, T. L.; Lopez, G. P. Control of Molecular Transport through Stimuli-Responsive Ordered Mesoporous Materials. *Adv. Mater.* **2003**, *15*, 1262–1266.
27. Tleugabulova, D.; Sui, J.; Ayers, P. W.; Brennan, J. D. Evidence for Rigid Binding of Rhodamine 6G to Silica Surfaces in Aqueous Solution Based on Fluorescence Anisotropy Decay Analysis. *J. Phys. Chem. B* **2005**, *109*, 7850–7858.
28. Tleugabulova, D.; Brennan, J. D. Quantifying Surface Coverage of Colloidal Silica by a Cationic Peptide Using a Combined Centrifugation/Time-Resolved Fluorescence Anisotropy Approach. *Langmuir* **2006**, *22*, 1852–1857.
29. Leng, X. J.; Starchev, K.; Buffle, J. Adsorption of Fluorescent Dyes on Oxide Nanoparticles Studied by Fluorescence Correlation Spectroscopy. *Langmuir* **2002**, *18*, 7602–7608.